blood

American Society of Hematology
2021 L Street NW, Suite 900,
Washington, DC 20036
Phone: 202-776-0544 | Fax 202-776-0545
editorial@hematology.org

Retinoid X receptor promotes hematopoietic stem cell fitness and quiescence and preserves hematopoietic homeostasis

Tracking no: BLD-2022-016832R1

María Piedad Menéndez-Gutiérrez (Centro Nacional de Investigaciones Cardiovasculares, Spain) Jesús Porcuna (Centro Nacional de Investigaciones Cardiovasculares, Spain) Ramesh Nayak (University of Cincinnati, United States) Ana Paredes (Centro Nacional de Investigaciones Cardiovasculares, Spain) Haixia Niu (Cincinnati Children's Hospital Medical Center, United States) Vanessa Núñez (Centro Nacional de Investigaciones Cardiovasculares, Spain) Aditi Paranjpe (Children's Hospital Medical Center, United States) Manuel J. Gómez (Centro Nacional de Investigaciones Cardiovasculares, Spain) Anukana Bhattacharjee (Cincinnati Children's Hospital Medical Center, United States) Daniel Schnell (Cincinnati Children's Hospital Medical Center, United States) Fátima Sánchez-Cabo (University of Cincinnati College of Medicine, United States) John S Welch (Washington University, United States) Nathan Salomonis (University of Cincinnati College of Medicine, United States) Jose Cancelas (University of Cincinnati College of Medicine, United States) Mercedes Ricote (Centro Nacional de Investigaciones Cardiovasculares, Spain)

Abstract:
Hematopoietic stem cells (HSCs) balance self-renewal and differentiation to maintain hematopoietic fitness throughout life. In steady-state conditions, HSC exhaustion is prevented by the maintenance of most HSCs in a quiescent state, with cells entering the cell cycle only occasionally. HSC quiescence is regulated by retinoid and fatty-acid ligands of transcriptional factors of the nuclear retinoid X receptor (RXR) family. Here, we show that dual deficiency for hematopoietic RXRa and RXRb induces HSC exhaustion, myeloid cell/megakaryocyte differentiation, and myeloproliferative-like disease. RXRa and RXRb maintain HSC quiescence, survival, and chromatin compaction; moreover, transcriptome changes in RXRa;RXRb-deficient HSCs include premature acquisition of an aging-like HSC signature, MYC pathway upregulation, and RNA intron retention. Fitness loss and associated RNA transcriptome and splicing alterations in RXRa;RXRb-deficient HSCs are prevented by *Myc* haploinsufficiency. Our study reveals the critical importance of RXRs for the maintenance of HSC fitness and their protection from premature aging.

Conflict of interest: No COI declared

COI notes:

Preprint server: No;

Author contributions and disclosures: Conceptualization: M.P.M-G., J.P., J.W., J.A.C. and M.R.; Methodology: M.P.M-G, J.P., R.N., A.P., H.N., and V.N.; Software: R.N., M.J.G., A.Pr., A. B., D.J.S, F. S-C and N.S.; Data interpretation and analysis: M.P.M-G., J.P., R.N., A.Pr., H.N., and M.J.G; Writing, reviewing & manuscript editing: M.P.M-G., J.P., J.W., N.S., J.A.C., and M.R.; Project supervision: J.A.C. and M.R.; Funding: J.A.C. and M.R.

Non-author contributions and disclosures: No;

Agreement to Share Publication-Related Data and Data Sharing Statement: Detailed material, datasets and protocols will be provided upon request. All the transcriptomic data has been deposited in the National Center for Biotechnology Information's Gene Expression Omnibus with the following accession numbers: GSE191163 and GSE199937.

Clinical trial registration information (if any):

Retinoid X receptor promotes hematopoietic stem cell fitness and quiescence and preserves hematopoietic homeostasis

Running title: RXR regulates hematopoietic stem cell fitness

María Piedad Menéndez-Gutiérrez,[1]* Jesús Porcuna,[1]* Ramesh Nayak,[3] Ana Paredes,[1] Haixia Niu,[3] Vanessa Núñez,[1] Aditi Paranjpe,[4] Manuel J. Gómez,[2] Anukana Bhattacharjee,[4] Daniel J. Schnell,[4] Fátima Sánchez-Cabo,[2] John S. Welch,[5] Nathan Salomonis,[4-6] José A. Cancelas,[3-7+] and Mercedes Ricote[1-8+]

[1]Myocardial Pathophysiology Area, [2]Bioinformatics Unit; Centro Nacional de Investigaciones Cardiovasculares (CNIC), Madrid, Spain.
[3]Stem Cell Program, Division of Experimental Hematology and Cancer Biology, [4]Division of Biomedical Informatics; Cincinnati Children's Hospital Medical Center, Cincinnati, Ohio, USA.
[5]Department of Internal Medicine, Washington University, St Louis, Missouri, USA
[6]Department of Pediatrics, University of Cincinnati College of Medicine, Cincinnati, Ohio, USA.
[7]Hoxworth Blood Center, University of Cincinnati College of Medicine, Cincinnati, Ohio, USA.
[8]Lead Contact

* These authors contributed equally

[+]Correspondence to: mricote@cnic.es; Jose.Cancelas@cchmc.org

Phone numbers: +34 914531200 ext 3306; +1 513-558-1324

Text word count: 4,364; Abstract word count: 147; Number of figures: 7; Number of references: 71

Scientific category: Hematopoiesis and stem cells

Key points

-RXRs are ligand-activated transcriptional units needed for the maintenance of HSC fitness, and preservation of a balanced hematopoiesis.

-RXRα;RXRβ-deficient HSCs transition from a dormant to a transcriptionally- and proliferative-active state through MYC pathway activation.

Abstract

Hematopoietic stem cells (HSCs) balance self-renewal and differentiation to maintain hematopoietic fitness throughout life. In steady-state conditions, HSC exhaustion is prevented by the maintenance of most HSCs in a quiescent state, with cells entering the cell cycle only occasionally. HSC quiescence is regulated by retinoid and fatty-acid ligands of transcriptional factors of the nuclear retinoid X receptor (RXR) family. Here, we show that dual deficiency for hematopoietic RXRα and RXRβ induces HSC exhaustion, myeloid cell/megakaryocyte differentiation, and myeloproliferative-like disease. RXRα and RXRβ maintain HSC quiescence, survival, and chromatin compaction; moreover, transcriptome changes in RXRα;RXRβ-deficient HSCs include premature acquisition of an aging-like HSC signature, MYC pathway upregulation, and RNA intron retention. Fitness loss and associated RNA transcriptome and splicing alterations in RXRα;RXRβ-deficient HSCs are prevented by *Myc* haploinsufficiency. Our study reveals the critical importance of RXRs for the maintenance of HSC fitness and their protection from premature aging.

Keywords

Retinoid X receptor, hematopoiesis, hematopoietic stem cells, HSC fitness, alternative splicing, MYC pathway.

Introduction

Hematopoietic stem cell (HSC) self-renewal and differentiation are subject to tight transcriptional regulation.[1] Features such as altered transcriptional programs, cellular stress, or age can impair HSC fitness and performance.[2,3] HSC fitness loss and exhaustion are associated with a gradual decline in HSC regenerative capacity, leading to an expansion of functionally weakened HSCs with an altered multi-lineage differentiation potential.[4,5]

Retinoid X receptors (RXRs) are members of the nuclear receptor (NR) superfamily of ligand-dependent transcription factors (TFs)[6] that respond to vitamin A derivatives (retinoids) and some endogenous fatty acids (FAs).[7] RXRs are encoded by three genes, *Rxra* (NR2B1), *Rxrb* (NR2B2), and *Rxrg* (NR2B3), which show time-specific and tissue-dependent differential expression. RXRs control pleiotropic genetic programs such as cell proliferation and differentiation, immune functions, and lipid and glucose metabolism by forming homodimers and heterodimers with others NRs, including other

retinoid-activated receptors, the retinoic acid receptors (RARs).[6] Retinoid-activated receptors are an attractive therapeutic target because of their ability to induce neutrophil differentiation.[8-10] However, their specific role in HSC maintenance and survival remains controversial, with conflicting results obtained with mice *versus* human HSCs.[10-13] Recent studies with retinoid-supplementation and retinoid-deprivation models demonstrated that retinoid signaling is essential for the regulation of HSC dormancy.[5,14] Since retinoids activate both the RARs and RXRs, some of the effects observed in these studies are likely driven by RXRs. Pharmacological approaches using RXR ligands suggest the importance of RXRs in HSC self-renewal and myeloid differentiation *in vitro,*[15,16] although off-target effects and the inability to generate complete loss-of-function models have hampered the interpretation of these experiments. To date no definitive genetic evidence has confirmed the role of the RXRs in HSC activity, since deficiency of individual RXR isoforms results in compensatory activity.[17] Here, we demonstrate that double deletion of *Rxra* and *Rxrb* leads to a decline in HSC fitness, characterized by HSC proliferative activation and exhaustion, and concomitant development of myeloproliferative-like disease (MPD). This phenotype derives from loss of HSC quiescence and self-renewal, openness of HSC chromatin, aberrant transcriptional splicing with increased intron retention, and activation of the signaling pathway controlled by MYC.[18] Using a model of Myc haploinsufficiency, we demonstrate that the loss of quiescence and altered transcription and splicing in RXR-deficient HSCs are mediated by MYC pathway activation. Our results provide definitive evidence that RXRs regulate HSC fitness and lineage fate by preserving transcriptional repression of the self-renewal master regulator MYC, and open new perspectives on the development of therapeutic approaches to prevent or reverse loss of HSC fitness.

Material and methods

Mice

Details of the generation and crossings of the animals used are provided in supplemental Materials and Methods.

Cell isolation

Cell isolation procedures are detailed in supplemental Materials and Methods.

Flow cytometry and cell sorting

Procedures for flow cytometry and cell sorting are described in supplemental Materials and Methods.

Colony forming unit-cell assays

CFU-cell assays were performed as detailed in supplemental Materials and Methods.

OP9NL1 co-cultures

OP9NL1 co-cultures were performed as detailed in supplemental Materials and Methods.

Generation of hematopoietic chimeras

Hematopoietic chimeras were generated as detailed in supplemental Materials and Methods.

CFSE-based homing assay

The procedures for homing assays are detailed in supplemental Materials and Methods.

5-FU assay

5-FU assays were performed as detailed in supplemental Materials and Methods.

Immunohistochemistry

Immunohistochemistry approaches are detailed in supplemental Materials and Methods.

HSC first division fate analysis

The procedures for first division fate analysis are described in supplemental Materials and Methods.

Quantitative real time PCR (Q-PCR)

Q-PCR experiments were performed as detailed in supplemental Materials and Methods.

Single cell RNA-seq processing and analysis

10x Genomics Chromium 3' v2 assay standard protocols were as previously described,[19] with minor modifications detailed in supplemental Materials and Methods.

Bulk, deep (b)RNA-seq processing and analysis

bRNA-seq assays are detailed in supplemental Materials and Methods.

Chromatin profiling by assay for transposase-accessible chromatin with sequencing (ATAC-Seq)

ATAC-seq was done as previously described,[20] with minor modifications detailed in supplemental Materials and Methods.

Cleavage under target and release using nuclease sequencing (CUT&RUNseq) assay

CUT&RUN assays were performed following published methods[21] with minor modifications, as detailed in supplemental Materials and Methods.

Serial competitive repopulation of Myc haploinsufficient HSCs

Serial competitive repopulation assays are described in supplemental Materials and Methods.

Statistical analysis

Statistical procedures are described in supplemental Materials and Methods.

Data Sharing

Transcriptomic data are deposited in the National Center for Biotechnology Information's Gene Expression Omnibus, with the following accession numbers: GSE191163, and GSE199937.

Results

Dual deletion of RXRα and RXRβ in the hematopoietic compartment causes expansion of the multipotential and myeloid progenitor cell pools

Transcript expression analysis of bone marrow (BM) hematopoietic cell subsets revealed ubiquitous *Rxra* and *Rxrb* expression in hematopoietic stem and multipotential progenitor cells (HSC/Ps; LSKs), including long-term (LT)-HSCs, short-term (ST)-HSCs, and multipotent progenitors (MPP2 and MPP3/MPP4)[22], as well as in committed erythro-myeloid progenitors (Lineage$^-$Sca-1$^-$c-kit$^+$ cells; LKs), including common myeloid (CMPs), granulocyte-monocyte (GMPs), and erythroid-megakaryocyte progenitors (MEPs) (Figures S1A-B). In all these hematopoietic populations, *Rxrg* expression was undetectable (C_T values ≥ 35). We inactivated RXRα or RXRβ in the HSC/Ps of neonatal pI:pC-inducible Mx-1^{Cre} transgenic mice[23] (Figure S2A). Postnatal deletion of RXRα (*Mx-1^{Cre+}Rxra$^{fl/fl}$* mice) or RXRβ (*Mx-1^{Cre+}Rxrb$^{fl/fl}$* mice) in HSC/Ps was insufficient to substantially alter hematopoiesis (Figures S2B-G, and Table S1). However, the deletion of both RXR isoforms (*Mx-1^{Cre+}Rxrab$^{fl/fl}$* mice) led to paler bones, reduced BM cellularity, splenomegaly, T-cell lymphopenia, and neutrophilia (Figures 2SA-B and Table S1). *Mx-1^{Cre+}Rxrab$^{fl/fl}$* mice also had significantly elevated numbers of eosinophils and LSKs in BM, reduced T cell numbers in PB and spleen, and significantly elevated numbers of spleen LSKs, LKs, and mature myeloid cells (Figures S2C-G). Thus, lack of RXRα;RXRβ in HSC/Ps leads to an expansion of multipotential and myeloid progenitor populations and to lymphopenia.

RXRα;RXRβ-deficient mice develop fatal myeloproliferative disease featuring prominent extramedullary hematopoiesis

To specifically delete *Rxra* and *Rxrb* in the hematopoietic compartment from embryonic stages onwards, we used the pan-hematopoietic Vav^{Cre} mouse model.[24] This resulted in loss of *Rxra* and *Rxrb* expression in HSC/Ps (Figure S3A) with no compensatory upregulation of *Rxrg* (C_T values ≥ 35). Analysis of hematopoietic parameters over two years revealed extramedullary hematopoiesis in

Vav^{Cre+}*Rxrab*$^{fl/fl}$ mice, shown by an early increase in spleen to body-weight ratio, a progressive rise in liver-to body weight ratio, and a later reduction in BM cellularity (Figures 1A-C and S3B). PB analysis of young *Vav*$^{Cre+}$*Rxrab*$^{fl/fl}$ mice revealed thrombocytosis (Figures 1D), lymphocytopenia, neutrophilia, and monocytosis (Figure 1E), as well as mild microcytic anemia (Figures 1F and S3C) and reduced BM erythropoiesis (Figures 1G and S3D-E). *Vav*$^{Cre+}$*Rxrab*$^{fl/fl}$ mice also had significantly increased numbers of BM and spleen LSKs (Figures 1H-I) and of spleen LKs, neutrophils, eosinophils, and monocytes (Figures 1J and S3F-H). These animals also showed a significant reduction in the numbers of PB B and T lymphocytes and in the CD4:CD8 ratio (Figures S3I-J). All these hematopoietic alterations persisted, and in most cases were magnified in aged *Vav*$^{Cre+}$*Rxrab*$^{fl/fl}$ mice (Figures 1A-J and S3C-J). Approximately half of the *Vav*$^{Cre+}$*Rxrab*$^{fl/fl}$ mice died at around 80 weeks of age, whereas none of the WT mice had died at the study endpoint (Figure 1K). Necropsy of surviving 24-month-old *Vav*$^{Cre+}$*Rxrab*$^{fl/fl}$ mice revealed pale bones, pronounced splenomegaly, and enlarged yellow-milky lungs (Figure 1L). Histological studies of distal femurs revealed increased numbers of megakaryocytes with hyperlobulated nuclei and an absence of adipocytes, with 50% of *Vav*$^{Cre+}$*Rxrab*$^{fl/fl}$ mice also presenting increased reticulin fibrosis with no collagen deposition (Figures 1M and S4A). *Vav*$^{Cre+}$*Rxrab*$^{fl/fl}$ mice had enlarged spleens with altered architecture and increased numbers of megakaryocytes (Figures 1L,N), as well as an overabundance of liver and lung leukocytes (Figures 1O and S4B-D). Histopathologic changes in *Vav*$^{Cre+}$*Rxrab*$^{fl/fl}$ lung tissue included massive alveolar inflammatory infiltration, accumulation of lipid-laden cells, alveolar hemorrhage, and abundant crystal deposition (Figure 1O). Morphological analysis of PB smears showed no detectable blasts, immature myeloblasts, or erythroid precursors in *Vav*$^{Cre+}$*Rxrab*$^{fl/fl}$ mice. The histopathological data of *Vav*$^{Cre+}$*Rxrab*$^{fl/fl}$ marrow and extramedullary hematopoiesis fulfilled the criteria for murine MPD[25,26].

RXRα;RXRβ-deficient HSCs show myeloid–megakaryocyte skewing and impaired repopulating activity

Single-cell (sc)RNA-seq analysis of sorted BM LSKs identified 12 shared discrete prior-defined cell states[27], including presumptive HSC-MPP and MPP in distinct cell-cycle phases (Figures 2A and S5A-B). *Vav*$^{Cre+}$*Rxrab*$^{fl/fl}$ LSKs were enriched in mitotic-M-M-G1, eMono, proNeu-1, and LMPP clusters, whereas WT LSKs showed enrichment in the MPP$^{ler3\text{-}high}$ and HSC-MPP clusters (GO-Elite Fischer Exact p-value ≤ 1e-4) (Figure S5C). Subclustering of the HSC-MPP cluster detected four subsets, two of them enriched in *Vav*$^{Cre+}$*Rxrab*$^{fl/fl}$ cells: a) *Vwf*-enriched megakaryocyte-biased activated, cycling

HSCs (c1)[28], and b) high output cells corresponding to proliferative *Plac8* expressing LT-HSCs (c3)[29,30] (Figures 2B-D). In contrast, WT HSC-MPPs were enriched in *Car2*-positive high-output MPPs (c2)[27] (Figures 2B-D). Gene-set enrichment analysis of the four HSC-MPP subclusters identified enriched gene sets associated with HSC priming and activation[5,27,31] in $Va^{Cre+}Rxrab^{fl/fl}$ HSC-MPPs (Figure 2E). All HSC-MPP populations from $Vav^{Cre+}Rxrab^{fl/fl}$ mice showed upregulation of MYC-dependent mRNA transcripts (e.g. *Cdk6* and *S100a6*),[32,33] and downregulation of genes associated with nonsense-mediated decay (Figure 2E).

FACS analysis of BM LSKs according to the expression of CD34 and the FLT3 receptor ('34F' HSCs)[34] and of CD48 and CD150 ('SLAM' HSCs)[22,35] revealed expansion of the most primitive HSC population ($CD34^{neg}FLT3^{neg}$ and $CD150^{+}CD48^{neg}$ LT-HSCs), myeloid-biased MPPs ($CD150^{+}CD48^{+}$ MPP2),[22] and $CD150^{neg}CD48^{+}$ cells containing both myeloid-biased MPP3[22] and lymphoid-primed MPP4[22] (Figures 2F,G,K, and S6A-C). However, $Vav^{Cre+}Rxrab^{fl/fl}$ BM showed significant depletion of downstream lymphoid-committed progenitors (CLPs) (Figures 2H and S6D), whereas there was an expansion of $CD41^{+}$ LT-HSCs (considered primed HSCs that accumulate with age[36] and have short-term—and primarily myeloid—regenerative potential[37]) and megakaryocyte-committed progenitors[38] (Figures 2I-K and S5H). Consistently, functional assays of BM progenitors revealed a marked increase in the numbers of megakaryocyte/myeloid CFUs, a decrease of pre-B CFUs (Figures 2L-M), and a reduction in stroma-dependent T-cell output (OP9NL1/BM co-cultures; Figures 2N and S6F-G). Analysis of PB CFUs revealed significantly higher numbers of CFU-G and CFU-GM in $Vav^{Cre+}Rxrab^{fl/fl}$ mice (Figures S6H-I), suggesting mobilization of myeloid-biased HSCs from BM to secondary hematopoietic organs. These data demonstrate that most expanded HSC/P subsets in $Vav^{Cre+}Rxrab^{fl/fl}$ mice were phenotypic LT-HSCs and myeloid–megakaryocyte progenitors with *in vitro* colony-forming ability.

We studied the repopulation capacity of WT and $Vav^{Cre+}Rxrab^{fl/fl}$ HSC/Ps, both alone or with a WT competitor[39] (Figures 3A and S7A). Analysis of PB cell chimerism revealed abnormal repopulation of $Vav^{Cre+}Rxrab^{fl/fl}$ HSC/Ps at each time interval (Figures 3B and S7B), with an especially marked decline in T lymphocyte reconstitution (Figures 3C and S7C). In addition, BM and spleen HSC/P chimerism was significantly diminished when $Vav^{Cre+}Rxrab^{fl/fl}$ BM cells were transplanted with a WT competitor (Figure 3C). We then analyzed the homing capacity of HSCs after intravenous injection of WT or $Vav^{Cre+}Rxrab^{fl/fl}$ BM or $c\text{-}kit^{+}$ cells into lethally irradiated mice, observing a significantly

reduced homing of *Vav*$^{Cre+}$*Rxrab*$^{fl/fl}$ BM progenitors and HSCs (Figures 3D-F and S7D-F). We analyzed the long-term reconstitution capacity of HSCs by serially transferring BM cells through primary and secondary WT recipients. To avoid engraftment defects, we used *Mx-1*$^{Cre+}$*Rxrab*$^{fl/fl}$ or WT mice as BM donors and induced *Rxra/Rxrb* deletion by intraperitoneal administration of pI:pC at 4 weeks post-transplantation (Figure S7G-H). Although primary recipients had comparable numbers of HSC/Ps regardless of donor genotype (data not shown), secondary recipients of *Mx-1*$^{Cre+}$*Rxra*b$^{fl/fl}$ BM had significantly fewer HSC/Ps than recipients of WT BM (Figure S7I). As a more rigorous test of HSC fitness, a limiting number of HSCs from WT *or* *Vav*$^{Cre+}$*Rxrab*$^{fl/fl}$ mice was co-transplanted with radioprotection-depleted WT LKs into irradiated mice (Figure 3G). Of the irradiated animals transplanted with *Vav*$^{Cre+}$*Rxrab*$^{fl/fl}$ HSCs, 90% died after the second week post-transplantation (Figure 3H), indicating that *Vav*$^{Cre+}$*Rxrab*$^{fl/fl}$ HSCs were deprived of hematopoietic radioprotection activity. Accordingly, colony replating assays revealed that *Vav*$^{Cre+}$*Rxrab*$^{fl/fl}$ HSCs lost their self-renewal capacity, whereas activation of RXRs with the retinoid 9c-RA enhanced their replating capacity (Figures 3I-J). These results indicate that RXRs have a cell-autonomous effect on HSCs fitness, and that loss of RXRs severely compromises the capacity of HSCs to home and radioprotect.

Quiescent HSCs transition to an active proliferative state in the absence of RXRs

To understand the role of RXRs in HSC/P proliferation, we performed a baseline *in vivo* BrdU pulse, demonstrating that *Vav*$^{Cre+}$*Rxrab*$^{fl/fl}$ LSKs and LT-HSCs progress faster than their WT counterparts through the cell-cycle S phase (Figure 4A). Pyronin Y coupled to Hoescht33342 labeling indicated that *Vav*$^{Cre+}$*Rxrab*$^{fl/fl}$ LSKs and LT-HSCs had higher cell-cycle activity and fewer G_0 phase cells than their WT counterparts, indicating loss of quiescence by RXRα;RXRβ-deficient HSC/Ps (Figure 4B). In addition, Annexin-V/DAPI labeling assays showed reduced frequencies of *Vav*$^{Cre+}$*Rxrab*$^{fl/fl}$ LSKs and LKs entering apoptosis (Figure S7J-K).

We treated *Vav*$^{Cre+}$*Rxrab*$^{fl/fl}$ and WT mice with 5-fluorouracil (5-FU) and tracked stressed hematopoietic recovery over 20 days (Figure 4C). Early (day 10-18) neutrophil and platelet recoveries were significantly delayed in *Vav*$^{Cre+}$*Rxrab*$^{fl/fl}$ mice (Figure 4D), confirming a fitness deficit in the response of RXRα;RXRβ-deficient HSCs. However, *Vav*$^{Cre+}$*Rxrab*$^{fl/fl}$ myeloid cells showed higher proliferative capacity in the late recovery phase, as shown by a significantly higher rebound than WT on post-treatment days 18 to 20 (2.15 ± 0.75 *versus* 1.26 ± 0.40 fold change, p = 0.0055), with this effect especially pronounced for monocytes (4.24 ± 2.61 *versus* 1.14 ± 0.87 fold change; p = 0.0034)

(Figure 4D). The frequencies of BM LT-HSCs and MPPs were higher in *Vav*$^{Cre+}$*Rxrab*$^{fl/fl}$ mice on post-treatment day 20 (Figure 4E), and BrdU labeling revealed higher proliferation rates of *Vav*$^{Cre+}$*Rxrab*$^{fl/fl}$ LSKs and LT-HSCs on post 5-FU treatment day 5 (Figure 4F-G). These results indicate that RXRα;RXRβ expression is required for the maintenance of HSCs quiescence and death rate in steady-state and stress hematopoiesis.

RXRα;RXRβ-deficient HSCs have an aged-like gene signature and show MYC signaling pathway activation and alternative splicing with intron retention

We performed a bulk (b)RNA-sequencing analysis on LT-HSCs and MPPs from five-month-old WT and *Vav*$^{Cre+}$*Rxrab*$^{fl/fl}$ mice. Analysis of the predominant gene expression patterns identified uniquely expressed transcripts in each of the separate captures (Figure 5A). While gene expression differed between *Vav*$^{Cre+}$*Rxrab*$^{fl/fl}$ LT-HSCs and MPPs and their WT counterparts, the greatest between-sample differences were by cell-state rather than genotype. This observation was further supported by principal component analysis of detectable genes, which showed that the major source of variance (PC1, 47%) was cell-state, with PC2 corresponding to genotype (Figure 5B). *Vav*$^{Cre+}$*Rxrab*$^{fl/fl}$ LT-HSCs were characterized by predominant upregulation of gene expression (fold change [FC] ≥ 1.5 or ≤ -1.5, adjusted p [p-adj] ≤ 0.1) (Figure 5C and Tables S2-3). In contrast, *Vav*$^{Cre+}$*Rxrab*$^{fl/fl}$ MPPs showed prominent transcript downregulation *versus* WT MPPs (fold change [FC] ≥ 1.5 or ≤ -1.5, adjusted p [p-adj] ≤ 0.1) (Figure S8A and Tables S4-5). Top downregulated genes in *Vav*$^{Cre+}$*Rxrab*$^{fl/fl}$ LT-HSCs included molecules important for lymphoid and erythroid development and function (*Klf9* and *Sptb*)[40,41] and *Pdk4*, which is essential for LT-HSC cell-cycle quiescence and metabolism[42] (Figure 5C and Tables S2-3).

Gene ontology analysis revealed that downregulated pathways in *Vav*$^{Cre+}$*Rxrab*$^{fl/fl}$ LT-HSCs were associated with splicing activity and erythrocyte development, whereas enriched pathways included cell–cell adhesion and leukocyte function (Figures S8B-C). In *Vav*$^{Cre+}$*Rxrab*$^{fl/fl}$ MPPs, upregulated pathways were related to oxidative stress, whereas downregulated pathways included TNFα and IL-6 production and T-cell activation (Figures S8B-C). Differentially-expressed genes (DEGs) in *Vav*$^{Cre+}$*Rxrab*$^{fl/fl}$ LT-HSCs included genes previously reported to be deregulated in aged HSCs[43] (Figure 5D). Other DEGs in *Vav*$^{Cre+}$*Rxrab*$^{fl/fl}$ LT-HSCs included MYC targets[44] and RNA processing and splicing genes (Figure 5D). To determine whether RNA splicing alterations might be involved in the aged-HSC signature of *Vav*$^{Cre+}$*Rxrab*$^{fl/fl}$ LT-HSCs, we analyzed novel splicing events

and intron retention.[31,45,46] This analysis identified 1,841 unique known and novel alternative splicing events differentiating WT from *Vav*$^{Cre+}$*Rxrab*$^{fl/fl}$ LT-HSCs, and 1,638 event differentiating WT from *Vav*$^{Cre+}$*Rxrab*$^{fl/fl}$ MPPs (empirical Bayes moderated t-test p<0.05) (Figure 5E). By considering inclusion (exon/intron gain) and exclusion (exon/intron loss) separately, we found that most events involved differential intron retention, preferentially in *Vav*$^{Cre+}$*Rxrab*$^{fl/fl}$ LT-HSCs (Figure 5E). Alternative splicing specific to *Vav*$^{Cre+}$*Rxrab*$^{fl/fl}$ LT-HSCs was associated with programmed cell death (e.g., *Madd*), cell-cycle arrest (e.g., *Araf*), chromatin modification (e.g., *Araf*), NR-mediated signaling (e.g., *Carm1*), thiol-ester hydrolase activity (e.g., *Usp20*), and cell–cell communication (e.g, *Itga5*); these findings were verified by genomic read visualization (Figure 5F). Significantly regulated splicing inclusion events in *Vav*$^{Cre+}$*Rxrab*$^{fl/fl}$ LT-HSCs were enriched in genes linked to GTPase activity and cell death, whereas significantly regulated exclusion splicing events were enriched in genes involved in the cell cycle, autophagy, and stress response control (Gene Ontology) (Figure S8D).

To generate a genome-wide profile of RXR binding in LT-HSCs and MPPs, we performed RXRα CUT&RUN assays. This analysis identified > 4,045 binding sites in LT-HSCs and > 13,070 RXR binding sites in MPPs, with sites preferentially located in promoter and upstream regions (Figures 5G and S8E, and Tables S6-7). Overlap analysis with bRNA-seq data demonstrated that a high number of DEGs in *Vav*$^{Cre+}$*Rxrab*$^{fl/fl}$ cells were directly regulated by RXRs (Figures 5H and S8F). Motif analysis of LT-HSC RXR peaks indicated enrichment for RXR binding sites and for motifs essential for the maintenance and differentiation of HSCs, including ETS-domain TFs (ETV4),[47] SP1,[48] and ATF3[49] (Figure 5I). Similar data were obtained in MPPs (Figure S8G). Functional annotation clustering analysis of the RXR cistrome identified a variety of enriched pathways in LT-HSCs and MPPs, including cell cycle and the MYC pathway, as well as processes involved in mRNA processing and splicing (Figures 5J and S8H). Our results provide evidence that RXRs function as master TFs that maintain a young-like HSC transcriptional signature, low MYC-dependent transcriptional activity, and appropriate splicing in LT-HSCs.

RXR deficiency leads to chromatin openness at promoter and enhancer regions in LT-HSCs

Assay for transposase-accessible chromatin with sequencing (ATAC-seq) revealed a strong spike in chromatin-accessible peaks in *Vav*$^{Cre+}$*Rxrab*$^{fl/fl}$ *versus* WT LT-HSCs (z score ≤ -2 or ≥ 2, p value ≤ 0.05) (Figure 6A and Tables S8-9), indicating that RXRα;RXRβ deficiency leads to chromatin openness in LT-HSCs. In contrast, *Vav*$^{Cre+}$*Rxrab*$^{fl/fl}$ MPPs had a higher proportion of closed peaks than

WT MPPs (FC ≤ -2 or ≥ 2, FDR ≤ 0.05) (Figure 6A and Tables S10-11). Analysis of peak distribution demonstrated a reorganization of the chromatin landscape in *Vav*$^{Cre+}$*Rxrab*$^{fl/fl}$ LT-HSCs but not MPPs (Figures S9A-B). Motif enrichment analysis showed a reduction in peaks enriched in binding sites for NRs in *Vav*$^{Cre+}$*Rxrab*$^{fl/fl}$ LT-HSCs and MPPs (p-value ≤0.01; Figures 6B and S9C). Conversely, *Vav*$^{Cre+}$*Rxrab*$^{fl/fl}$ LT-HSCs were highly enriched in binding sites for several TFs with roles in hematopoiesis, including the master hematopoiesis regulators GATA1, 2, and 3[50] and Runx1[51]; Meis1, which is overexpressed in certain leukemias[52]; the myeloid differentiation master TF PU.1[53]; and the HSC-activity marker HOX9A[54] (Figure 6B). Similar binding-site enrichment was found in *Vav*$^{Cre+}$*Rxrab*$^{fl/fl}$ MPPs (Figure S9C). Overlap analysis between RXR-binding sites and *Vav*$^{Cre+}$*Rxrab*$^{fl/fl}$ *versus* WT differentially accessible regions (DARs) revealed that around 50% of changes in MPP chromatin accessibility were RXR-dependent, whereas a lower proportion of DARs co-localized with RXR-binding sites in LT-HSCs (Figures S9D-E).

We performed CUT&RUN assays to determine the monomethylation and trimethylation status of lysine 4 (H3K4me1 and H3K4me3) and the acetylation status of lysine 27 (H3K27ac) in histone 3 (Figure S9F). An overlap analysis between open DARs and regions marked by i) high H3K4me3 and H3K27Ac (located ± 1 kb from a TSS; putative promoters), ii) high H3K4me1 and H3K27Ac (located > 1 kb and < -1 kb from a TSS; putative active enhancers), and iii) high H3K4me1 but no H3K27Ac(located > 1 kb and < -1 kb from a TSS; putative poised enhancers) revealed that most open DARs in *Vav*$^{Cre+}$*Rxrab*$^{fl/fl}$ LT-HSCs coincided with active promoters and enhancers (Figure 6C). Double H3K4me3;H3K27Ac- and/or H3K4me1;H3K27Ac-enriched regions overlapping with RXR-binding sites and DARs were found in *loci* harboring HSC-aging signature genes,[43] leukemia oncogenes, MYC targets, and RNA processing genes, including *Flt3*, *Lmo1*, *Dhrs3*, *Cdk6*, *Snrpd3*, and *Fxr2* (Figure 6D). These data indicate that RXRs contribute to the LT-HSCs maintenance of chromatin condensation and transcriptional repression, which are hallmarks of cell quiescence.[55]

Myc haploinsufficiency rescues regeneration of phenotypically identifiable LT-HSCs in RXR-deficient mice

To determine if MYC mediates the role of RXRs in HSC fitness, we crossed *Myc*-haploinsufficient mice[56] with *Vav*$^{Cre+}$*Rxrab*$^{fl/fl}$ mice, generating *Vav*$^{Cre+}$*Rxrab*$^{fl/fl}$-*Myc*$^{+/fl}$ mice. The functional capacities of equal numbers of BM HSC/Ps from WT, *Vav*$^{Cre+}$*Rxrab*$^{fl/fl}$, or *Vav*$^{Cre+}$*Rxrab*$^{fl/fl}$-*Myc*$^{+/fl}$ mice were tested in competitive repopulation assays (Figures 7A and S10A). Although the PB donor contribution of

333 *Vav*$^{Cre+}$*Rxrab*$^{fl/fl}$-*Myc*$^{+/fl}$ mice was even lower than that of *Vav*$^{Cre+}$*Rxrab*$^{fl/fl}$ mice (Figure S10B), *Myc*
334 haploinsuficiency rescued the regeneration of LT-HSCs (but not other HSC/Ps) (Figures 7B and
335 S10C). Cell-cycle analysis showed that *Myc* haploinsufficiency restored the level of *Vav*$^{Cre+}$*Rxrab*$^{fl/fl}$ LT-
336 HSCs in G_0 phase and the percentage of proliferating cells back to WT levels (Figures 7C-D). We
337 performed a pair-daughter first HSC division assay, in which MYC upregulation in daughter cells is a
338 hallmark of loss of self-renewing divisions.[57,58] Lack of RXRs entailed a ~2 fold increase in the
339 frequency of differentiated/committed daughter cells, concomitant with a reduction in symmetric self-
340 renewal division modes (Figures 7E-F). These changes in fate division were restored to WT levels in
341 *Vav*$^{Cre+}$*Rxrab*$^{fl/fl}$-*Myc*$^{+/fl}$ mice (Figures 7E-F). The rescue of self-renewing cells was also observed *in*
342 *vitro* by serial plating analysis (Figure 7G). However, *Myc* haploinsufficiency did not restore the pre-B-
343 cell progenitor content in BM (Figure S10D).

344 Next, we performed bRNA-seq in WT, *Vav*$^{Cre+}$*Rxrab*$^{fl/fl}$ and *Vav*$^{Cre+}$*Rxrab*$^{fl/fl}$-*Myc*$^{+/fl}$ LT-HSCs.
345 Analyses of these data show that *Myc* haploinsufficiency partially restores *Vav*$^{Cre+}$*Rxrab*$^{fl/fl}$
346 transcriptional (40%) and splicing (13%) defects (Figures 7H-L and S10E, and Tables S12-15).
347 Rescued DEGs included diverse transcriptional regulators (e.g., *Gfi1 and Irf7*), and few RNA-binding
348 proteins (e.g., *RnaseI,* and *Snapc4*) (Figure 7I). Although only a small percentage of RXR-dependent
349 splicing events were rescued (Figures 7J-L), 62% of them were enriched in the reversal of intron-
350 retention in genes involved in post-transcriptional regulation (e.g. *Sf1* and *U2af2*), regulation of
351 translation (e.g. *Tcea2* and *Ago2*), chromatin DNA binding (e.g. *Tox* and *Per1*), and transcriptional
352 regulation (e.g. *Sp100* and *Setd6*) (Figure 7K). Our results demonstrate that MYC activity is the key
353 RXR-dependent molecular regulator of LT-HSC fitness, *in vivo* regeneration activity, as well as
354 transcriptome and spliceosome.
355

356 **Discussion**

357 In this study, we demonstrate that RXRs are essential for the maintenance of HSC activity and
358 balanced hematopoietic differentiation. Dual lack of RXRα and RXRβ in HSCs leads to chromatin
359 openness and the acquisition of a premature aged-like transcriptional and phenotypic signature in LT-
360 HSCs. As a result, these cells transition from a dormant to a proliferative and transcriptionally active
361 state characterized by MYC activity upregulation and intron retention, which lead to the exhaustion of
362 functional HSCs. This manifests in lymphopenia and a myeloid/megakaryocyte-skewed hematopoietic

system in RXRα;RXRβ-deficient mice that eventually progresses to fatal MPD in the context of myeloproliferation-associated inflammation and hemostatic defects similar to those observed in other mouse models of fatal MPD.[26,59]

Chromatin openness and transcriptional activation of RXRα;RXRβ-deficient HSCs contrasts the transcriptional downregulation and reduced chromatin accessibility of RXRα;RXRβ-deficient committed cells, suggesting that the mechanisms driving RXR control over HSC quiescence and lineage choice are cell-context dependent. The complexity of mechanisms that can be controlled by RXRs might be explained by their promiscuity; RXRs regulate several NRs via direct dimerization and binding of cognate ligands and coactivators, as demonstrated in other cell types (reviewed in[60]). Our TF motif analysis indicates that RXR/RAR binding sites are overrepresented in the LT-HSC signature, pointing to RXR/RAR signaling as an important player in RXR-mediated control of HSC fitness.[5] Accordingly, recent studies demonstrated that vitamin-A signaling, and especially non-classical retinoid signaling mediated by CYP26B1 and 4-oxo-RA, regulates the dormancy and long-term repopulation capacity of mouse HSCs through RXR/RARβ.[14] The cell-autonomous mechanism of this regulatory path may be species-specific, since *Cyp29b1* is expressed in mouse HSCs while in humans it is expressed in BM niche but not HSC cells.[13,14] Our study supports a role for RXRs in mouse HSC fitness beyond their collaborative role in RXR/RARβ heterodimers. Considering that RXRs play an active role in response to retinoids,[61] remaining transcriptional effects in *Rarb*-KO HSCs treated with retinoids[14] might be explained by RARβ-independent RXR activation. In addition, although both *Rarb*- and *Cyp26b1*-deficient mice present diminished HSC self-renewal capacities[14], none of these mice recapitulate the profound phenotype of RXRα;RXRβ-deficient mice. For example, unlike RXRα;RXRβ-deficient LT-HSCs, HSC lacking non-classical retinoid signaling retain radioprotection ability. This suggests that signaling pathways other than retinoids contribute to the role of RXRs in the control of LT-HSC fitness. Several recent research lines point to FAs as RXR ligands that provide a metabolic link to HSC biology. FA metabolism is specifically enriched in LT-HSCs relative to progenitor cells.[14] Importantly, we identified the long-chain FA C24:5 as a natural ligand of RXRs in HSCs, both under basal and stressed hematopoiesis.[62] Moreover, FA metabolism is upregulated in HSCs from old mice[63], and HSC functionality is recovered after treatment with y-linoleic acid in both aged humans and mice.[63] Thus, although RA seems to have different effects in humans and mice,[13,64] HSC responses to FA treatment are similar in both species. Future studies could explore whether

combination of a retinoid with FAs could improve *ex vivo* expansion of human HSCs and offer a route toward stem-cell gene therapy.

Another important finding is that the loss of one *Myc* allele prevented the loss of quiescence and self-renewal, *in vivo* regeneration capacity, and the changes in the transcriptional and splicing regulatory landscapes of RXRα;RXRβ-deficient HSCs. Our results demonstrate that MYC activity lies at the root of the HSC phenotype associated with loss of RXR signaling. Interestingly, a normal distribution of progeny downstream of LT-HSCs was not restored, suggesting that MYC is indispensable for the initial phase of LT-HSC fate commitment but not for differentiation in later divisions. This is in agreement with previous studies demonstrating that MYC expression is very low in dormant HSCs but increases during the transition toward active HSCs and subsequently multipotent progenitors.[5] Beyond the known role of MYC in the control of self-renewal,[65] our results suggest that MYC signaling activation in RXRα;RXRβ-deficient HSCs promotes a phenotype compatible with HSC aging through the control of alternative splicing, leading to global intron retention.[66,67] The mechanisms by which MYC carries out this transcriptional activity might direct or indirect. MYC activation has the potential to impact HSC fitness, since alterations to ribosomal biogenesis and RNA splicing contribute to age-associated HSC epigenetic reprogramming[68] and to myelodysplastic-related disorders and leukaemia.[69,70] Our results demonstrate that lack of RXRα;RXRβ in HSCs triggers a spike in intron retention in LT-HSCs, with extensive alteration to genes and processes involved in mRNA processing and splicing, through a MYC-dependent mechanism. Despite intense biological research over several decades, pharmacological inhibition of MYC remains ineffective due to its "undruggable" protein structure.[71] Our study points to RXRs as potential druggable targets for maintaining HSC fitness during transplantation procedures and protecting against premature HSC aging and MPD.

Acknowledgments

We thank the members of the J.A.C. and M.R. laboratories for extensive discussions and critiques of the manuscript. We thank Daniel Metzger (Université de Strasbourg, France) for *Rxrb*$^{f/f}$ mice, Juan Carlos Zúñiga-Pflücker (Sunnybrook Health Sciences Centre, Canada) for OP9-NL1 cells, Daniel Jiménez-Carretero (CNIC) for t-SNE analysis, the CRG (Barcelona, Spain) Genomics Unit for ATAC-seq sequencing, and S. Bartlett (CNIC) for editorial assistance. We also thank the staff of the CNIC Cellomics and Animal facilities for technical support. This study was supported by grants from the

Spanish Ministerio de Ciencia e Innovación (MICIN) (SAF2017-90604-REDT-NurCaMein, RTI2018-095928-B100, and PID2021-122552OB-I00), La Marató de TV3 Foundation (201605-32), and the Comunidad de Madrid (MOIR-B2017/BMD-3684) to M.R and from the Formación de Profesorado Universitario (FPU17/01731) program (MICIN) to J.P. The project also received funding from the US National Institutes of Health (R01 DK124115, P01 HL158688, R01 HL147536, R01 CA237016 and U54 DK126108 to J.A.C). The CNIC is supported by the Instituto de Salud Carlos III (ISCIII), the Ministerio de Ciencia e Innovación (MCIN), and the Pro CNIC Foundation and is a Severo Ochoa Center of Excellence (grant CEX2020-001041-S funded by MICIN/AEI/10.13039/501100011033).

Author Contributions

Conceptualization: M.P.M-G., J.P., J.W., J.A.C. and M.R.; Methodology: M.P.M-G, J.P., R.N., A.P., H.N., and V.N.; Software: R.N., M.J.G., A.Pr., A. B., D.J.S, F. S-C and N.S.; Data interpretation and analysis: M.P.M-G., J.P., R.N., A.Pr., H.N., and M.J.G; Writing, reviewing & manuscript editing: M.P.M-G., J.P., J.W., N.S., J.A.C., and M.R.; Project supervision: J.A.C. and M.R.; Funding: J.A.C. and M.R.

Conflict Of Interest Disclosures

The authors declare no competing interests.

References

1. Cabezas-Wallscheid N, Klimmeck D, Hansson J, et al. Identification of regulatory networks in HSCs and their immediate progeny via integrated proteome, transcriptome, and DNA methylome analysis. *Cell Stem Cell*. 2014;15(4):507-522.
2. Kruta M, Sunshine MJ, Chua BA, et al. Hsf1 promotes hematopoietic stem cell fitness and proteostasis in response to ex vivo culture stress and aging. *Cell Stem Cell*. 2021;28(11):1950-1965 e1956.
3. Akunuru S, Geiger H. Aging, Clonality, and Rejuvenation of Hematopoietic Stem Cells. *Trends Mol Med*. 2016;22(8):701-712.
4. Zhang Y, Wong J, Klinger M, Tran MT, Shannon KM, Killeen N. MLL5 contributes to hematopoietic stem cell fitness and homeostasis. *Blood*. 2009;113(7):1455-1463.
5. Cabezas-Wallscheid N, Buettner F, Sommerkamp P, et al. Vitamin A-Retinoic Acid Signaling Regulates Hematopoietic Stem Cell Dormancy. *Cell*. 2017;169(5):807-823 e819.
6. Rőszer T, Menendez-Gutierrez MP, Cedenilla M, Ricote M. Retinoid X receptors in macrophage biology. *Trends Endocrinol Metab*. 2013;24(9):460-468.

7. Krezel W, Ruhl R, de Lera AR. Alternative retinoid X receptor (RXR) ligands. *Mol Cell Endocrinol*. 2019;491:110436.

8. Gratas C, Menot M-L, Dresch D, Chomienne C. Retinoic acid supports granulocytic but not erythrocytic differentiation of myeloid progenitors in normal bone marrow. *Leukemia*. 1993;7:1156-1162.

9. Labrecque J, Allan D, Chambon P, Iscove NN, Lohnes D, Hoang T. Impaired granulocytic differentiation in vitro in hematopoietic cells lacking retinoic acid receptors alpha1 and gamma. *Blood*. 1998;92(2):607-615.

10. Purton LE, Bernstein ID, Collins SJ. All-trans retinoic acid delays the differentiation of primitive hematopoietic precursors (lin-c-kit+Sca-1(+)) while enhancing the terminal maturation of committed granulocyte/monocyte progenitors. *Blood*. 1999;94(2):483-495.

11. Chute JP, Muramoto GG, Whitesides J, et al. Inhibition of aldehyde dehydrogenase and retinoid signaling induces the expansion of human hematopoietic stem cells. *Proc Natl Acad Sci U S A*. 2006;103(31):11707-11712.

12. Purton LE, Bernstein ID, Collins SJ. All-trans retinoic acid enhances the long-term repopulating activity of cultured hematopoietic stem cells. *Blood*. 2000;95(2):470-477.

13. Ghiaur G, Yegnasubramanian S, Perkins B, Gucwa JL, Gerber JM, Jones RJ. Regulation of human hematopoietic stem cell self-renewal by the microenvironment's control of retinoic acid signaling. *Proc Natl Acad Sci U S A*. 2013;110(40):16121-16126.

14. Schonberger K, Obier N, Romero-Mulero MC, et al. Multilayer omics analysis reveals a non-classical retinoic acid signaling axis that regulates hematopoietic stem cell identity. *Cell Stem Cell*. 2021.

15. Safi R, Muramoto GG, Salter AB, et al. Pharmacological manipulation of the RAR/RXR signaling pathway maintains the repopulating capacity of hematopoietic stem cells in culture. *Mol Endocrinol*. 2009;23(2):188-201.

16. Sakashita A, Kizaki M, Pakkala S, et al. 9-cis-retinoic acid: effects on normal and leukemic hematopoiesis in vitro. *Blood*. 1993;81(4):1009-1016.

17. Ricote M, Snyder CS, Leung HY, Chen J, Chien KR, Glass CK. Normal hematopoiesis after conditional targeting of RXRalpha in murine hematopoietic stem/progenitor cells. *J Leukoc Biol*. 2006;80(4):850-861.

18. Delgado MD, Leon J. Myc roles in hematopoiesis and leukemia. *Genes Cancer*. 2010;1(6):605-616.

19. Salomonis N. Investigating Cell Fate Decisions with ICGS Analysis of Single Cells. *Methods Mol Biol*. 2019;1975:251-275.

20. Buenrostro JD, Wu B, Chang HY, Greenleaf WJ. ATAC-seq: A Method for Assaying Chromatin Accessibility Genome-Wide. *Curr Protoc Mol Biol*. 2015;109:21 29 21-29.

21. Skene PJ, Henikoff JG, Henikoff S. Targeted in situ genome-wide profiling with high efficiency for low cell numbers. *Nat Protoc*. 2018;13(5):1006-1019.

22. Pietras EM, Reynaud D, Kang YA, et al. Functionally Distinct Subsets of Lineage-Biased Multipotent Progenitors Control Blood Production in Normal and Regenerative Conditions. *Cell Stem Cell*. 2015;17(1):35-46.

23. Kühn R, Schwenk F, Aguet M, Rajewsky K. Inducible gene targeting in mice. *Science*. 1995;269:1427-1429.

24. de Boer J, Williams A, Skavdis G, et al. Transgenic mice with hematopoietic and lymphoid specific expression of Cre. *Eur J Immunol*. 2003;33(2):314-325.

25. Kogan SC, Ward JM, Anver MR, et al. Bethesda proposals for classification of nonlymphoid hematopoietic neoplasms in mice. *Blood*. 2002;100(1):238-245.

26. Thomas EK, Cancelas JA, Chae HD, et al. Rac guanosine triphosphatases represent integrating molecular therapeutic targets for BCR-ABL-induced myeloproliferative disease. *Cancer Cell*. 2007;12(5):467-478.

27. Rodriguez-Fraticelli AE, Weinreb C, Wang SW, et al. Single-cell lineage tracing unveils a role for TCF15 in haematopoiesis. *Nature*. 2020;583(7817):585-589.

28. Carrelha J, Meng Y, Kettyle LM, et al. Hierarchically related lineage-restricted fates of multipotent haematopoietic stem cells. *Nature*. 2018;554(7690):106-111.

29. Regan-Komito D, Swann JW, Demetriou P, et al. GM-CSF drives dysregulated hematopoietic stem cell activity and pathogenic extramedullary myelopoiesis in experimental spondyloarthritis. *Nat Commun*. 2020;11(1):155.

30. Zhang YH, Hu Y, Zhang Y, Hu LD, Kong X. Distinguishing three subtypes of hematopoietic cells based on gene expression profiles using a support vector machine. *Biochim Biophys Acta Mol Basis Dis*. 2018;1864(6 Pt B):2255-2265.

31. Muench DE, Ferchen K, Velu CS, et al. SKI controls MDS-associated chronic TGF-beta signaling, aberrant splicing, and stem cell fitness. *Blood*. 2018;132(21):e24-e34.

32. Zhang J, Yang P, Liu D, et al. c-Myc Upregulated by High Glucose Inhibits HaCaT Differentiation by S100A6 Transcriptional Activation. *Front Endocrinol (Lausanne)*. 2021;12:676403.

33. Bretones G, Delgado MD, Leon J. Myc and cell cycle control. *Biochim Biophys Acta*. 2015;1849(5):506-516.

34. Spangrude GJ, Heimfeld S, Weissman IL. Purification and characterization of mouse hematopoietic stem cells. *Science*. 1988;241(4861):58-62.

35. Kiel MJ, Yilmaz OH, Iwashita T, Yilmaz OH, Terhorst C, Morrison SJ. SLAM family receptors distinguish hematopoietic stem and progenitor cells and reveal endothelial niches for stem cells. *Cell*. 2005;121(7):1109-1121.

36. Gekas C, Graf T. CD41 expression marks myeloid-biased adult hematopoietic stem cells and increases with age. *Blood*. 2013;121(22):4463-4472.

37. Bernitz JM, Daniel MG, Fstkchyan YS, Moore K. Granulocyte colony-stimulating factor mobilizes dormant hematopoietic stem cells without proliferation in mice. *Blood*. 2017;129(14):1901-1912.

38. Grisouard J, Shimizu T, Duek A, et al. Deletion of Stat3 in hematopoietic cells enhances thrombocytosis and shortens survival in a JAK2-V617F mouse model of MPN. *Blood*. 2015;125(13):2131-2140.
39. Taniguchi Ishikawa E, Chang KH, Nayak R, et al. Klf5 controls bone marrow homing of stem cells and progenitors through Rab5-mediated beta1/beta2-integrin trafficking. *Nat Commun*. 2013;4:1660.
40. Zhang Y, Xue Y, Cao C, et al. Thyroid hormone regulates hematopoiesis via the TR-KLF9 axis. *Blood*. 2017;130(20):2161-2170.
41. Ekblom M. Expression of spectrin in normal and malignant erythropoiesis. *Scand J Haematol*. 1984;33(4):378-385.
42. Takubo K, Nagamatsu G, Kobayashi CI, et al. Regulation of glycolysis by Pdk functions as a metabolic checkpoint for cell cycle quiescence in hematopoietic stem cells. *Cell Stem Cell*. 2013;12(1):49-61.
43. Flohr Svendsen A, Yang D, Kim K, et al. A comprehensive transcriptome signature of murine hematopoietic stem cell aging. *Blood*. 2021;138(6):439-451.
44. Kim J, Lee JH, Iyer VR. Global identification of Myc target genes reveals its direct role in mitochondrial biogenesis and its E-box usage in vivo. *PLoS One*. 2008;3(3):e1798.
45. Fenix AM, Miyaoka Y, Bertero A, et al. Gain-of-function cardiomyopathic mutations in RBM20 rewire splicing regulation and re-distribute ribonucleoprotein granules within processing bodies. *Nat Commun*. 2021;12(1):6324.
46. Itskovich SS, Gurunathan A, Clark J, et al. MBNL1 regulates essential alternative RNA splicing patterns in MLL-rearranged leukemia. *Nat Commun*. 2020;11(1):2369.
47. Ciau-Uitz A, Wang L, Patient R, Liu F. ETS transcription factors in hematopoietic stem cell development. *Blood Cells Mol Dis*. 2013;51(4):248-255.
48. Gilmour J, O'Connor L, Middleton CP, et al. Robust hematopoietic specification requires the ubiquitous Sp1 and Sp3 transcription factors. *Epigenetics Chromatin*. 2019;12(1):33.
49. Liu Y, Chen Y, Deng X, Zhou J. ATF3 Prevents Stress-Induced Hematopoietic Stem Cell Exhaustion. *Front Cell Dev Biol*. 2020;8:585771.
50. Gao J, Chen YH, Peterson LC. GATA family transcriptional factors: emerging suspects in hematologic disorders. *Exp Hematol Oncol*. 2015;4:28.
51. Nottingham WT, Jarratt A, Burgess M, et al. Runx1-mediated hematopoietic stem-cell emergence is controlled by a Gata/Ets/SCL-regulated enhancer. *Blood*. 2007;110(13):4188-4197.
52. Unnisa Z, Clark JP, Roychoudhury J, et al. Meis1 preserves hematopoietic stem cells in mice by limiting oxidative stress. *Blood*. 2012;120(25):4973-4981.
53. Burda P, Laslo P, Stopka T. The role of PU.1 and GATA-1 transcription factors during normal and leukemogenic hematopoiesis. *Leukemia*. 2010;24(7):1249-1257.
54. Cabal-Hierro L, van Galen P, Prado MA, et al. Chromatin accessibility promotes hematopoietic and leukemia stem cell activity. *Nat Commun*. 2020;11(1):1406.
55. Swygert SG, Kim S, Wu X, et al. Condensin-Dependent Chromatin Compaction Represses Transcription Globally during Quiescence. *Mol Cell*. 2019;73(3):533-546 e534.

56. Sheng Y, Ma R, Yu C, et al. Role of c-Myc haploinsufficiency in the maintenance of HSCs in mice. *Blood*. 2021;137(5):610-623.
57. Cheng Y, Luo H, Izzo F, et al. m(6)A RNA Methylation Maintains Hematopoietic Stem Cell Identity and Symmetric Commitment. *Cell Rep*. 2019;28(7):1703-1716 e1706.
58. Althoff MJ, Nayak RC, Hegde S, et al. Yap1-Scribble polarization is required for hematopoietic stem cell division and fate. *Blood*. 2020;136(16):1824-1836.
59. Mullally A, Lane SW, Ball B, et al. Physiological Jak2V617F expression causes a lethal myeloproliferative neoplasm with differential effects on hematopoietic stem and progenitor cells. *Cancer Cell*. 2010;17(6):584-596.
60. De Bosscher K, Desmet SJ, Clarisse D, Estebanez-Perpina E, Brunsveld L. Nuclear receptor crosstalk - defining the mechanisms for therapeutic innovation. *Nat Rev Endocrinol*. 2020;16(7):363-377.
61. Di Martino O, Niu H, Hadwiger G, et al. Endogenous and combination retinoids are active in myelomonocytic leukemias. *Haematologica*. 2021;106(4):1008-1021.
62. Niu H, Fujiwara H, di Martino O, et al. Endogenous retinoid X receptor ligands in mouse hematopoietic cells. *Sci Signal*. 2017;10(503):eaan1011.
63. Dong S, Wang Q, Kao YR, et al. Chaperone-mediated autophagy sustains haematopoietic stem-cell function. *Nature*. 2021;591(7848):117-123.
64. Canete A, Cano E, Munoz-Chapuli R, Carmona R. Role of Vitamin A/Retinoic Acid in Regulation of Embryonic and Adult Hematopoiesis. *Nutrients*. 2017;9(2).
65. Wilson A, Murphy MJ, Oskarsson T, et al. c-Myc controls the balance between hematopoietic stem cell self-renewal and differentiation. *Genes Dev*. 2004;18(22):2747-2763.
66. Hsu TY, Simon LM, Neill NJ, et al. The spliceosome is a therapeutic vulnerability in MYC-driven cancer. *Nature*. 2015;525(7569):384-388.
67. Anczukow O, Krainer AR. The spliceosome, a potential Achilles heel of MYC-driven tumors. *Genome Med*. 2015;7:107.
68. Adelman ER, Huang HT, Roisman A, et al. Aging Human Hematopoietic Stem Cells Manifest Profound Epigenetic Reprogramming of Enhancers That May Predispose to Leukemia. *Cancer Discov*. 2019;9(8):1080-1101.
69. Yoshida K, Sanada M, Shiraishi Y, et al. Frequent pathway mutations of splicing machinery in myelodysplasia. *Nature*. 2011;478(7367):64-69.
70. Venkatasubramanian M, Chen X, Kashish Chetal M, et al. A Prognostic Human Splicing Signature That Precurses Leukemia. *Blood*. 2018;132(Supplement_1):877.
71. Chen H, Liu H, Qing G. Targeting oncogenic Myc as a strategy for cancer treatment. *Signal Transduct Target Ther*. 2018;3:5.

Figure legends

Figure 1. Vav^{Cre+}*Rxrab*$^{fl/fl}$ mice develop lethal myeloproliferative disorders. (A-C) Organ weight and counts of 2-, 5-, 12- and 24-month-old WT and *Vav*$^{Cre+}$*Rxrab*$^{fl/fl}$ mice. (A-B) Spleen and liver weigh-

to-body weight ratios. (C) BM cellularity per femur. (D-F) Hemogram data of 2-, 5-, 12- and 24-month-old WT and *Vav*$^{Cre+}$*Rxrab*$^{fl/fl}$ mice. (D) Mean platelet counts. (E) Percentage of lymphocytes, neutrophils and monocytes among white blood cells. (F) Total red blood cells. (G-J) Flow cytometry of femur and spleen homogenates from 2-, 5-, 12- and 24-month-old WT and *Vav*$^{Cre+}$*Rxrab*$^{fl/fl}$ mice. (G) Absolute numbers of erythroid progenitors (CD45^{neg}Ter119^{+} cells) per femur. (H) Absolute numbers of LSKs per femur. (I-J) Absolute numbers of spleen LSKs and LKs. (K) Kaplan-Meier survival plots for WT and *Vav*$^{Cre+}$*Rxrab*$^{fl/fl}$ mice (n = 11-13 per genotype). (L) Representative images of femurs, spleens, and lungs of 24-month-old WT and *Vav*$^{Cre+}$*Rxrab*$^{fl/fl}$ mice. (M-N) Representative images of H&E- and reticulin-stained femur sections, and of H&E-stained spleen sections from 24-month-old WT and *Vav*$^{Cre+}$*Rxrab*$^{fl/fl}$ mice; yellow arrows indicate megakaryocytes; Ad, adipocytes. Scale bars: 500 μm (N, upper panels), 100 μm (M, upper panels; N, bottom panels) or 50 μm (M, bottom panels). (O) Representative images of H&E-stained lungs from 24-month-old WT and *Vav*$^{Cre+}$*Rxrab*$^{fl/fl}$ mice; black arrows indicate alveolar hemorrhage; B, bronchiole; A, alveoli; AS, alveolar sac. Scale bars: 2.5 mm (left panels) or 250 μm (middle and right panels). Data are presented as mean ± *SEM*: (A-F) n = 7-17 mice, pooled from up to three independent experiments per age group and genotype; (G) n = 3-13 mice, pooled from up to two independent experiments per age group and genotype; (H) n = 4-24 mice, pooled from up to three independent experiments per age group and genotype; (I) n = 5-12, pooled from up to two independent experiments per age and genotype (spleen); (J) n = 5-11 mice, pooled from up to two independent experiments per age and genotype. Significance was determined by two-way ANOVA followed by Sidak's multiple comparisons test (aged-paired mice) (A-J), or log-rank (Mantel-Cox) test (K), and is represented as: *$p \leq 0.05$; **$p \leq 0.01$; ***$p \leq 0.001$; ****$p \leq 0.0001$.

Figure 2. Expansion of megakaryocyte–myeloid-biased stem cells in RXRα;RXRβ-deficient mice. (A-E) Single-cell (sc)RNA-seq (10x Genomics) of sorted LSKs from WT and *Vav*$^{Cre+}$*Rxrab*$^{fl/fl}$ BM cells (shown are clusters derived from gene-set enrichment of a compendium of prior HSC/P subsets from single-cell functional studies [Rodríguez-Fraticelli et al., 2000]). (A-B) UMAP plots of HSC/P subsets derived from *Vav*$^{Cre+}$*Rxrab*$^{fl/fl}$ and WT BM LSKs (A), and of subclustering of the broader HSC-MPP cluster (B). (C) Top HSC-MPP cluster marker genes. (D) HSC-MPP population frequencies, showing significant differences between *Vav*$^{Cre+}$*Rxrab*$^{fl/fl}$ and WT mice (Fischer Exact *p*-value thresholds are indicated). (E) Heatmap showing differentially expressed genes identified by

642 *cellHarmony* analysis of each HSC-MPP subcluster in *Vav*$^{Cre+}$*Rxrab*$^{fl/fl}$ *versus* WT mice. On the left of
643 the associated clusters are shown enriched prior-defined HSC/P functional subsets (blue), pathways
644 (pink), or curated transcription factor targets (green) (GO-Elite software); on the right of the associated
645 clusters are shown matching bRNA-Seq regulated genes. (F-K) Flow cytometry of BM from 5-month-
646 old WT and *Vav*$^{Cre+}$*Rxrab*$^{fl/fl}$ mice. (F-G) Absolute numbers of HSC subpopulations per femur,
647 according to the "34F" or "SLAM" stain codes. (H) Absolute numbers of CLPs per femur. (I) Frequency
648 of CD41^{+} and CD41^{neg} cells in the CD150^{+}CD48^{neg}LT-HSC subset. (J) Absolute numbers of MK
649 progenitor per femur. (K) Annotated t-SNE plots for the identified Lineage^{neg} BM-cell populations from
650 WT and *Vav*$^{Cre+}$*Rxrab*$^{fl/fl}$ mice using the "SLAM" stain code as in (G). Insets in the top panels show
651 magnifications of the plotted HSC/P subpopulations; plots in the lower panels show overlaid
652 biexponential transformed marker expression levels (n = 3-4 per genotype); CLP, common lymphoid
653 progenitor; HSC, hematopoietic stem cell; LT, long-term; MK, megakaryocyte; MPP, multipotent
654 progenitor; ST, short-term. (L-M) Colony-forming unit assay in total BM cells from 5-month-old WT and
655 *Vav*$^{Cre+}$*Rxrab*$^{fl/fl}$ mice. (L) Representative images of hematopoietic colonies identified in *Vav*$^{Cre+}$*Rxrab*$^{fl/fl}$
656 mice after 7 days of incubation: burst-forming unit-erythroid (BFU), unipotent CFU-M (monocyte),
657 CFU-MK (megakaryocyte), CFU-G (granulocyte) and CFU-pre-B (B lymphocyte) progenitors; bipotent
658 CFU-GM (granulocyte, monocyte) progenitors; and multipotent CFU-GEMM (granulocyte, erythrocyte,
659 monocyte, and megakaryocyte) progenitors. (M) Number of colonies per $20x10^3$ plated BM cells (n =
660 6; three mice per genotype, with two technical replicates per mouse; data are representative of two
661 independent experiments). (N) Lymphocyte output after 8 days of OP9NL1 cell co-culture with BM
662 cells from 5-month-old WT and *Vav*$^{Cre+}$*Rxrab*$^{fl/fl}$ mice; graph shows the percentage of T cells
663 (DN1+DN2+DN3+DN4+CD3^{+} cells, for gating strategy see Figure S6F) and Cd11b^{+} cells within CD45^{+}
664 lymphocytes. Data are shown as means ± *SEM*, and dots represent individual animals. Significance
665 was determined by unpaired Student t test, and is represented as: *$p \leq 0.05$; **$p \leq 0.01$; ***$p \leq 0.001$;
666 ****$p \leq 0.0001$; n.s. = not significant.
667
668 **Figure 3. RXRα;RXRβ-deficient HSCs are functionally defective.** (A-C) Competitive transplantation
669 assay (1:1 mix) of unfractionated BM cells from WT or *Va*$^{Cre+}$*Rxrab*$^{fl/fl}$ mice (CD45.2^{+}) and C57BL/6
670 mice (CD45.1^{+}) into lethally irradiated C57BL/6 mice (CD45.1^{+}) (data are representative of three
671 independent experiments). (A) Experimental design. (B) FACS analysis of the percentage of total

donor chimerism in PB 4, 8, 12, and 16 weeks after transplantation (n = 9-10). (C) FACS analysis of cell-specific chimerism in PB, BM and spleen 16 weeks after competitive repopulation assay. (D-F) Homing assay of total BM cells from WT or *Vav*$^{Cre+}$*Rxrab*$^{fl/fl}$ mice (CD45.2^{+}), transplanted into lethally irradiated C57BL/6 mice (CD45.1^{+}). (D) Experimental design. (E) Representative FACS plots showing the gating strategies for analysis of CD45.2^{+} HSCs. (F) Total numbers of CD45.2^{+} HSCs found in the BM of recipient mice. (G-H) Transplantation of purified LT-HSC from WT or *Vav*$^{Cre+}$*Rxrab*$^{fl/fl}$ mice (CD45.2^{+}) along with LKs from C57BL/6 mice (CD45.1^{+}) into lethally irradiated C57BL/6 mice (CD45.1^{+}) (n = 19-20, data pooled from two independent experiments). (G) Experimental design. (H) Kaplan-Meier survival plot. (I-J) Serial CFU plating assay after 48-h *in vitro* treatment of purified LT-HSCs from 5-month-old WT or *Vav*$^{Cre+}$*Rxrab*$^{fl/fl}$ mice with 9cRA or vehicle. (I) Experimental design. (J) Number of CFUs normalized to control vehicle treatment of each corresponding plating (data pooled from two independent experiments). All data are shown as means ± *SEM*, and dots represent individual animals. Significance was determined by two-way ANOVA followed by Sidak's multiple comparisons test (B), unpaired Student t test (C and F), Log-rank (Mantel-Cox) test (H), or ordinary one-way ANOVA (J), and is represented as: *$p \leq 0.05$; **$p \leq 0.01$; ***$p \leq 0.001$; ****$p \leq 0.0001$; n.s., not significant.

Figure 4. Dual lack of RXRα and RXRβ in HSCs leads to cell-cycle activation and quiescence exit. (A) Representative flow cytometry density plots showing BrdU incorporation by LSKs and CD150^{+}CD48^{neg} LT-HSCs after a 24 hour pulse (left); the plot (right) shows the frequencies of cells with BrdU incorporation (data are pooled from two independent experiments). (B) Representative flow cytometry density plots showing Pyronin Y and Hoescht33342 staining by LSKs and CD150^{+}CD48^{neg} LT-HSCs (up); plots (down) show frequencies of cells with double Pyronin Y and Hoescht33342 staining (data are pooled from two independent experiments). (C-E) Recovery of hematopoietic cells after 5-FU administration to *Vav*$^{Cre+}$*Rxrab*$^{fl/fl}$ and WT mice. (C) Experimental design. (D) Time course of PB-cell counts (baseline was defined as the mean reading on day 0, expressed as 100%; n = 9-11 mice per genotype). (E) Absolute HSC/P numbers in total BM 20 days after 5-FU administration. (F-H) HSC/P proliferation 5 days after 5-FU administration to *Vav*$^{Cre+}$*Rxrab*$^{fl/fl}$ and WT mice. (F) Experimental design. (G) Representative flow cytometry density plots showing BrdU incorporation by LSKs and CD150^{+}CD48^{neg} LT-HSCs. (H) Frequencies of BrdU-positive cells. All data are presented as means ±

SEM, and dots represent individual animals. Significance was determined by unpaired Student t test (A, B, E and H), or two-way ANOVA followed by Sidak's multiple comparisons test (D; aged-paired mice), and is represented as: *$p \leq 0.05$, **$p \leq 0.01$, ***$p \leq 0.001$, ****$p \leq 0.0001$; n.s., not significant.

Figure 5. Lack of RXRα and RXRβ provokes an HSC-aged signature, MYC signaling pathway activation, and intron retention in LT-HSCs. (A-F) Bulk transcriptome of WT and *Vav*$^{Cre+}$*Rxrab*$^{fl/fl}$ LT-HSCs and MPP BM cells. (A) Heatmap showing the top specific marker genes per sorted population/genotype, obtained with MarkerFinder software. (B) Principal component analysis (PCA) of the transcriptomes in (A). (C) Volcano plot showing the global transcriptional changes in *Vav*$^{Cre+}$*Rxrab*$^{fl/fl}$ *versus* WT LT-HSCs determined by bRNA-seq. Each circle represents one differentially-expressed gene (DEG), and colored circles represent DEGs showing significant upregulation (*p-adj* ≤ 0.1 and *FC* ≥ 1.5 [orange]), or significant downregulation (*p-adj* ≤ 0.1 and *FC* ≤ -1.5 [blue]). Normalized expression values from bRNA-seq data are provided in Table S2. (D) Heatmap showing normalized Log_2FC scores for the expression of HSC aging signature genes, MYC pathway genes, and RNA processing and splicing-related genes in WT and *Vav*$^{Cre+}$*Rxrab*$^{fl/fl}$ LT-HSCs. (E-F) Number of alternative splicing events in *Vav*$^{Cre+}$*Rxrab*$^{fl/fl}$ *versus* WT LT-HSCs and MPPs for distinct alternative exon and intron usage forms. Splicing events associated with exon or intron inclusion (increased relative expression) *versus* exclusion are shown separately for LT-HSC and MPP comparisons. (F) SashimiPlot read-level visualization of intron–retention-associated splicing events in WT (red) and *Vav*$^{Cre+}$*Rxrab*$^{fl/fl}$ (blue) bRNA-Seq LT-HSC samples. Exon–exon junction-spanning reads are denoted with curved lines, together with associated read counts. (G-J) RXRα whole genome binding (CUT&RUN- seq). (G) Genomic distribution of enriched regions in WT LT-HSCs identified in the RXR CUT&RUN data set. (H) Overlaps of total LT-HSC RXRα CUT&RUN peaks with bRNA-seq upregulated and dowregulated genes in *Vav*$^{Cre+}$*Rxrab*$^{fl/fl}$ *versus* WT LT-HSCs. (I) HOMER analysis of known motifs in WT LT-HSC RXRα peaks. (J) List of significantly enriched GO terms in WT LT-HSC promoters (± 1 kb from the transcription start site (TSS); black bars) and upstream regions (± 1 to 20 kb from the TSS; gray bar) for diverse pathways upon analysis of the RXRα CUT&RUN data set using the CCHMC ToppGene suite (https://toppgene.cchmc.org/enrichment.jsp) (FDR (B&H) ≤ 0.01).

Figure 6. Chromatin openness at enhancer and promoter sites in RXRα;RXRβ-deficient LT-HSCs. (A) Heatmap of ATAC-seq signals located in TSS-flanking regions (± 1 kb) in 5-month-old *Vav*$^{Cre+}$*Rxrab*$^{fl/fl}$ and WT LT-HSCs and MPPs. (B) HOMER known motif analysis of ATAC-seq peaks. The top panels shows transcription factor motifs enriched in WT LT-HSCs relative to the background of *Vav*$^{Cre+}$*Rxrab*$^{fl/fl}$ LT-HSC peaks. The bottom panel shows transcription factor motifs enriched in *Vav*$^{Cre+}$*Rxrab*$^{fl/fl}$ LT-HSCs relative to the background of WT LT-HSCs peaks. (C) Peak annotations identified in an overlap analysis between the open promoter and enhancer regions in LT-HSCs identified in the ATAC-seq experiment (defined by genomic distribution; see also Figure S8A), and regions marked by high H3K4me3 and H3K27Ac, and ± 1 kb from TSS (putative promoters), high H3K4me1 and H3K27Ac, and > 1 kb and < -1 kb from the TSS (putative active enhancers), and high H3K4me1 but no H3K27Ac, and > 1 kb and < -1 kb from the TSS (putative poised enhancers). (D) UCSC genome browser track examples of active enhancers (vertical gray highlights) and promoters (vertical blue highlights) within *loci* that overlap RXRα CUT&RUN and ATAC-seq peaks.

Figure 7. *Myc* haploinsufficiency rescues regeneration, transcriptome and spliceosome of phenotypically identifiable LT-HSCs. (A-B) Competitive transplantation assay of unfractionated BM cells from 4-month-old WT, *Vav*$^{Cre+}$*Rxrab*$^{fl/fl}$, and *Vav*$^{Cre+}$*Rxrab*$^{fl/fl}$-*Myc*$^{+/fl}$ mice (CD45.2^{+}) in a 1:1 ratio with C57BL/6 BM cells (CD45.1^{+}) into lethally irradiated C57BL/6 mice (CD45.1^{+}) (data pooled from two independent experiments). (A) Experimental scheme. (B) Percentages of CD45.2^{+} BM LT-HSCs at 16 weeks post-transplantation. (C) Frequencies of CD150^{+}CD48^{neg} LT-HSCs from WT, *Vav*$^{Cre+}$*Rxrab*$^{fl/fl}$, and *Vav*$^{Cre+}$*Rxrab*$^{fl/fl}$-*Myc*$^{+/fl}$ mice in the G_0 phase of the cell cycle (Pyronin Y^{neg}/Hoescht33342^{neg}; data pooled from three independent experiments). (D) Percentage of BrdU^{+} CD150^{+}CD48^{neg} LT-HSCs from WT, *Vav*$^{Cre+}$*Rxrab*$^{fl/fl}$, and *Vav*$^{Cre+}$*Rxrab*$^{fl/fl}$-*Myc*$^{+/fl}$ mice after 1 hour pulse with BrdU. (E-F) Immunofluorescence analysis, showing different division modes according to MYC expression in paired daughter LT-HSCs from WT, *Vav*$^{Cre+}$*Rxrab*$^{fl/fl}$, and *Vav*$^{Cre+}$*Rxrab*$^{fl/fl}$-*Myc*$^{+/fl}$ mice. (E) Representative images showing (1) symmetric self-renewal (absence of MYC expression in paired daughter cells), (2) asymmetric division (high *versus* low MYC expression in paired daughter cells), and (3) symmetric differentiation/commitment (MYC expression in both cells); scale bar, 10 µm. (F) Percentage of LT-HSCs corresponding to division modes 1, 2, and 3 as in (E); n=60 division pairs captured from five WT mice; n=48 division pairs captured from three *Vav*$^{Cre+}$*Rxrab*$^{fl/fl}$ mice; and n =37

761 division pairs captured from five *Vav*$^{Cre+}$*Rxrab*$^{fl/fl}$-*Myc*$^{+/fl}$ mice. Analyses were performed in two
762 independent experiments. (G) Serial CFU plating assay in total BM cells from WT, *Vav*$^{Cre+}$*Rxrab*$^{fl/fl}$, or
763 *Vav*$^{Cre+}$*Rxrab*$^{fl/fl}$-*Myc*$^{+/fl}$ mice. (H-L) Bulk transcriptome of WT, *Vav*$^{Cre+}$*Rxrab*$^{fl/fl}$, and *Vav*$^{Cre+}$*Rxrab*$^{fl/fl}$-
764 *Myc*$^{+/fl}$ LT-HSCs. Normalized expression values from bRNA-seq data are provided in Table S12-15.
765 (H) Rescued differentially expressed genes in *Vav*$^{Cre+}$*Rxrab*$^{fl/fl}$-*Myc*$^{+/fl}$ *versus* *Vav*$^{Cre+}$*Rxrab*$^{fl/fl}$ LT-HSCs
766 (eBayes t-test $p < 0.05$, fold > 1.2), compared to *Vav*$^{Cre+}$*Rxrab*$^{fl/fl}$-*Myc*$^{+/fl}$ *versus* WT LT-HSCs (eBayes
767 t-test $p < 0.05$, FDR corrected, fold > 1.5). (I) Heatmap of the 435 rescued genes showing silencing of
768 *Vav*$^{Cre+}$*Rxrab*$^{fl/fl}$ LT-HSC-induced transcripts by *Myc*$^{+/fl}$ expression. On the left are shown transcripts
769 called out from prior analyses (Fig. 5D, TFs, or RNA-binding regulators). (J) Rescued alternative
770 splicing events in *Vav*$^{Cre+}$*Rxrab*$^{fl/fl}$-*Myc*$^{+/fl}$ *versus* *Vav*$^{Cre+}$*Rxrab*$^{fl/fl}$ LT-HSCs, compared to
771 *Vav*$^{Cre+}$*Rxrab*$^{fl/fl}$-*Myc*$^{+/fl}$ versus WT LT-HSCs (eBayes t-test $p < 0.05$, $\delta PSI > 0.1$ for both comparisons).
772 (K) Heatmap of 154 unique splicing events, organized by increased junction percent spliced in (PSI)
773 value in *Vav*$^{Cre+}$*Rxrab*$^{fl/fl}$ *versus* WT LT-HSCs, with exemplar intron retention events (green tick mark)
774 and genes symbols called out. (L) Number of observed unique annotated splicing events in the 154
775 rescued splicing events, by exon/intron inclusion or exclusion. Splicing events associated with exon or
776 intron inclusion (increased relative expression) *versus* exclusion are shown separately. Results are
777 presented as means ± *SEM*, and dots represent individual animals. Significance was determined by
778 ordinary one-way ANOVA, and is represented as $*p \leq 0.05$, $**p \leq 0.01$, $***p \leq 0.001$, and n.s. = not
779 significant.

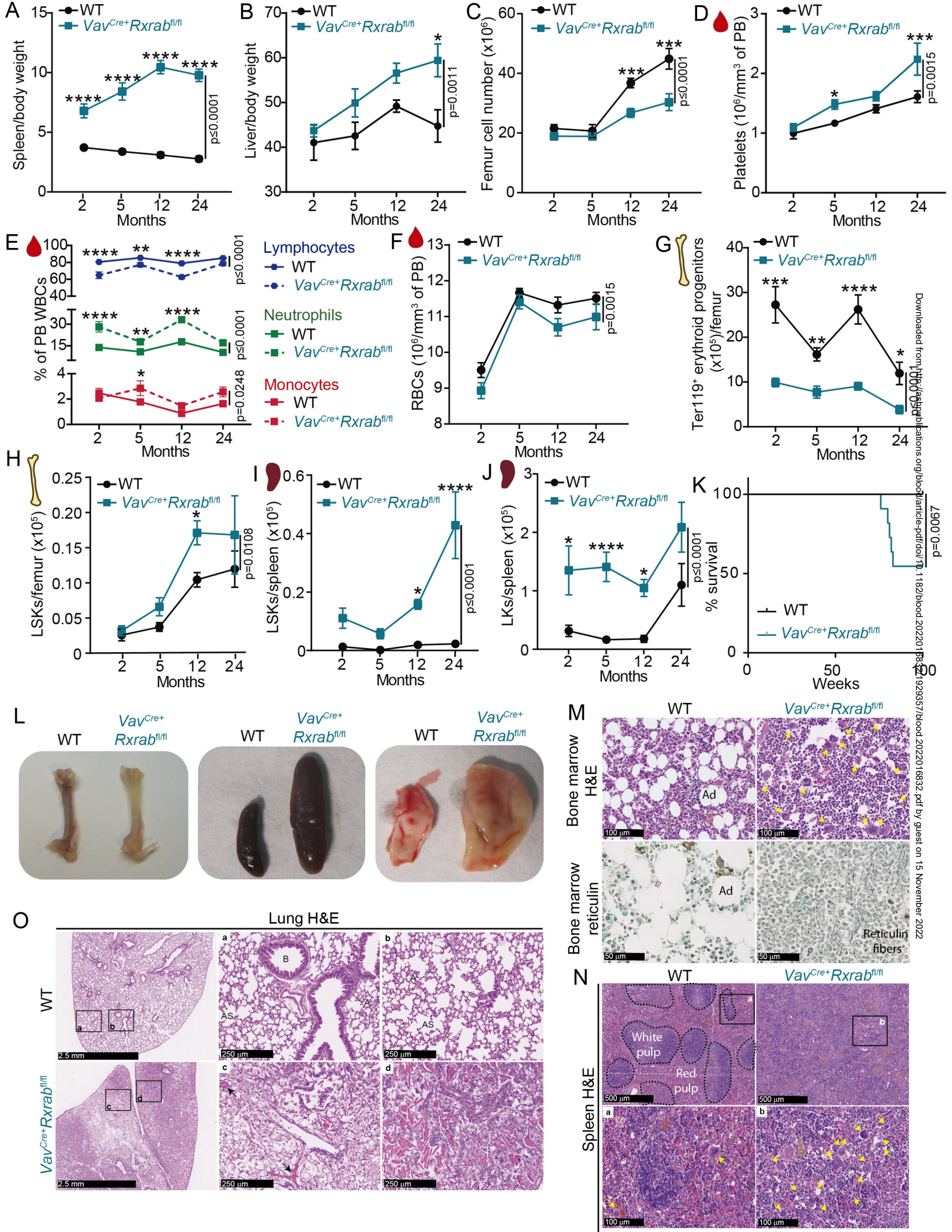

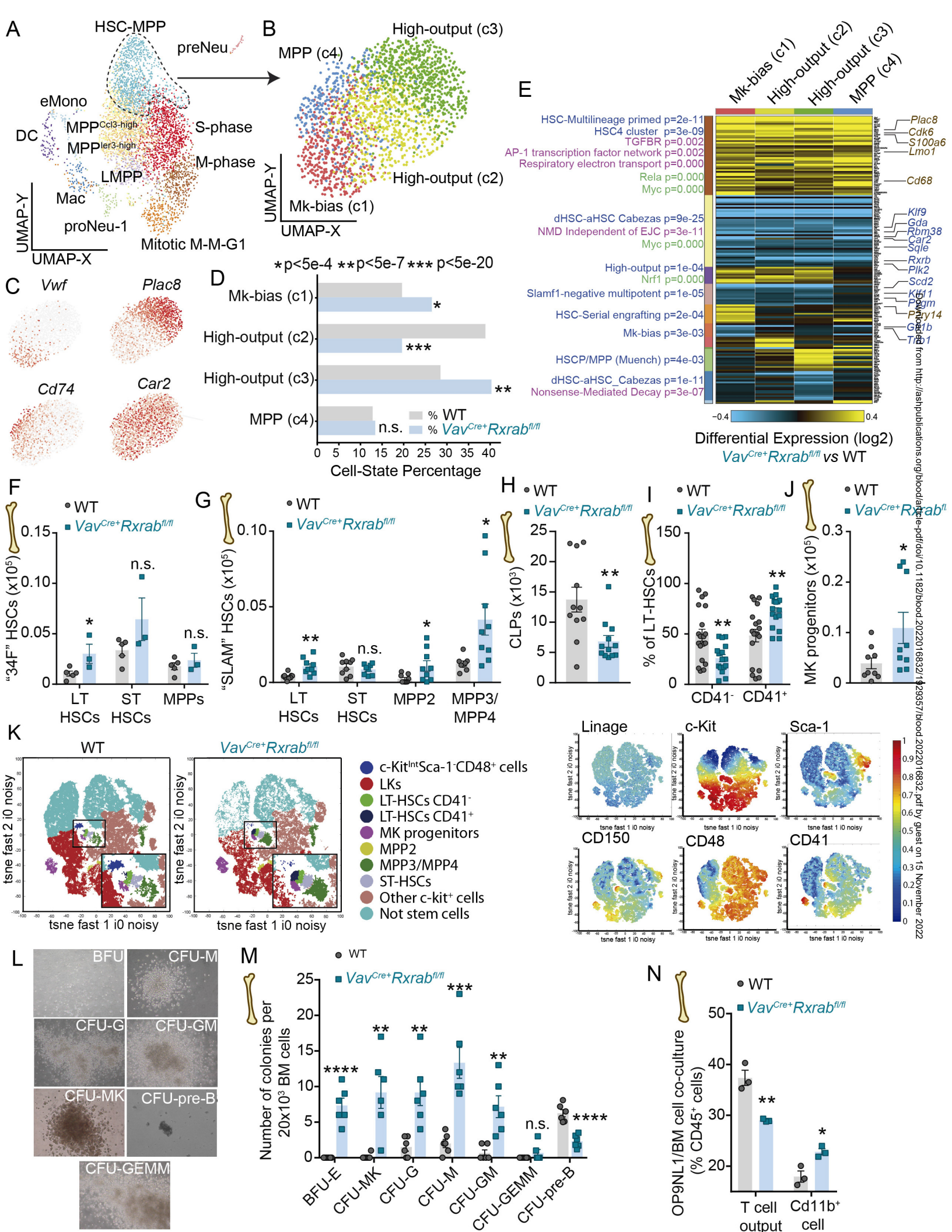

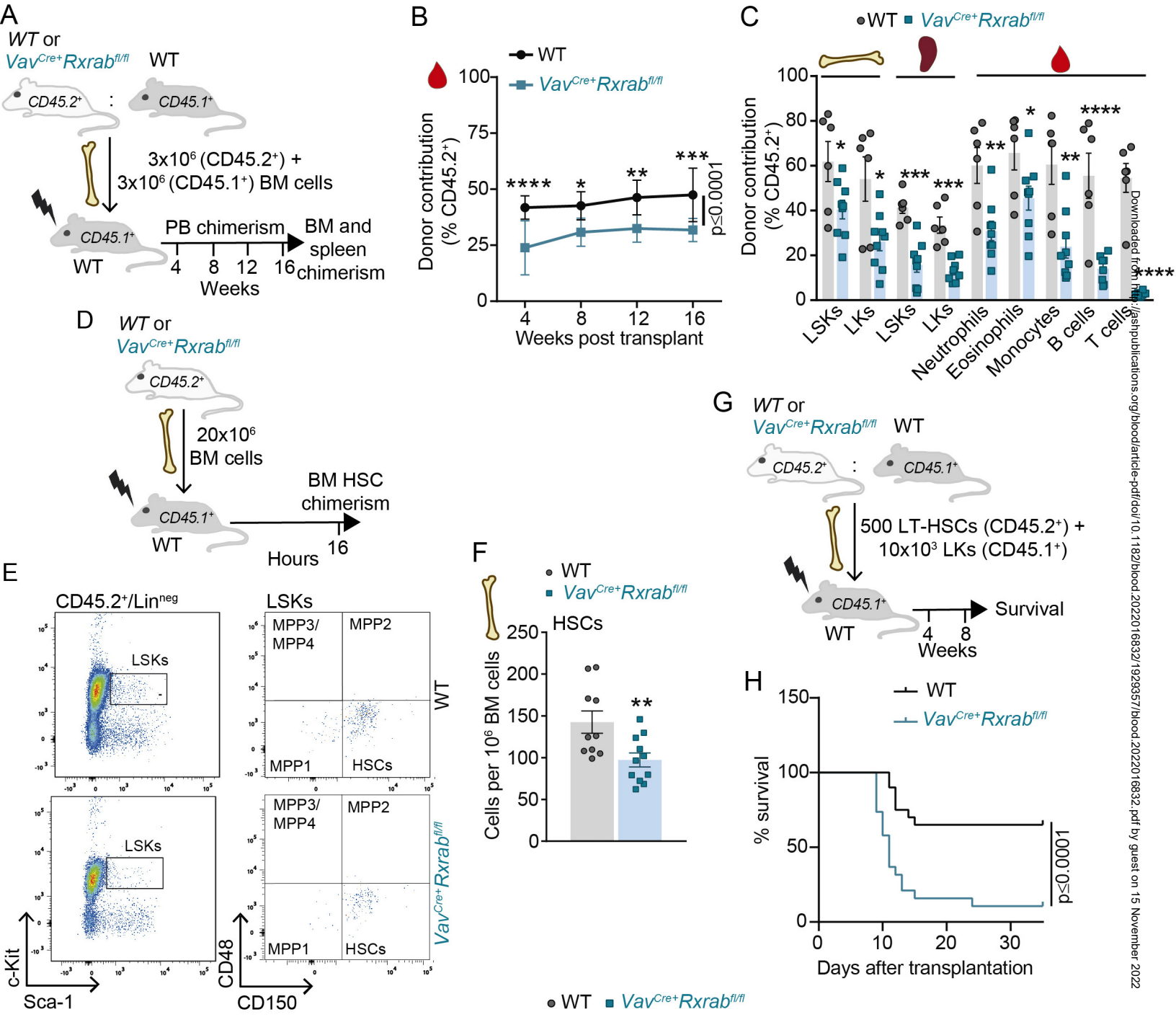

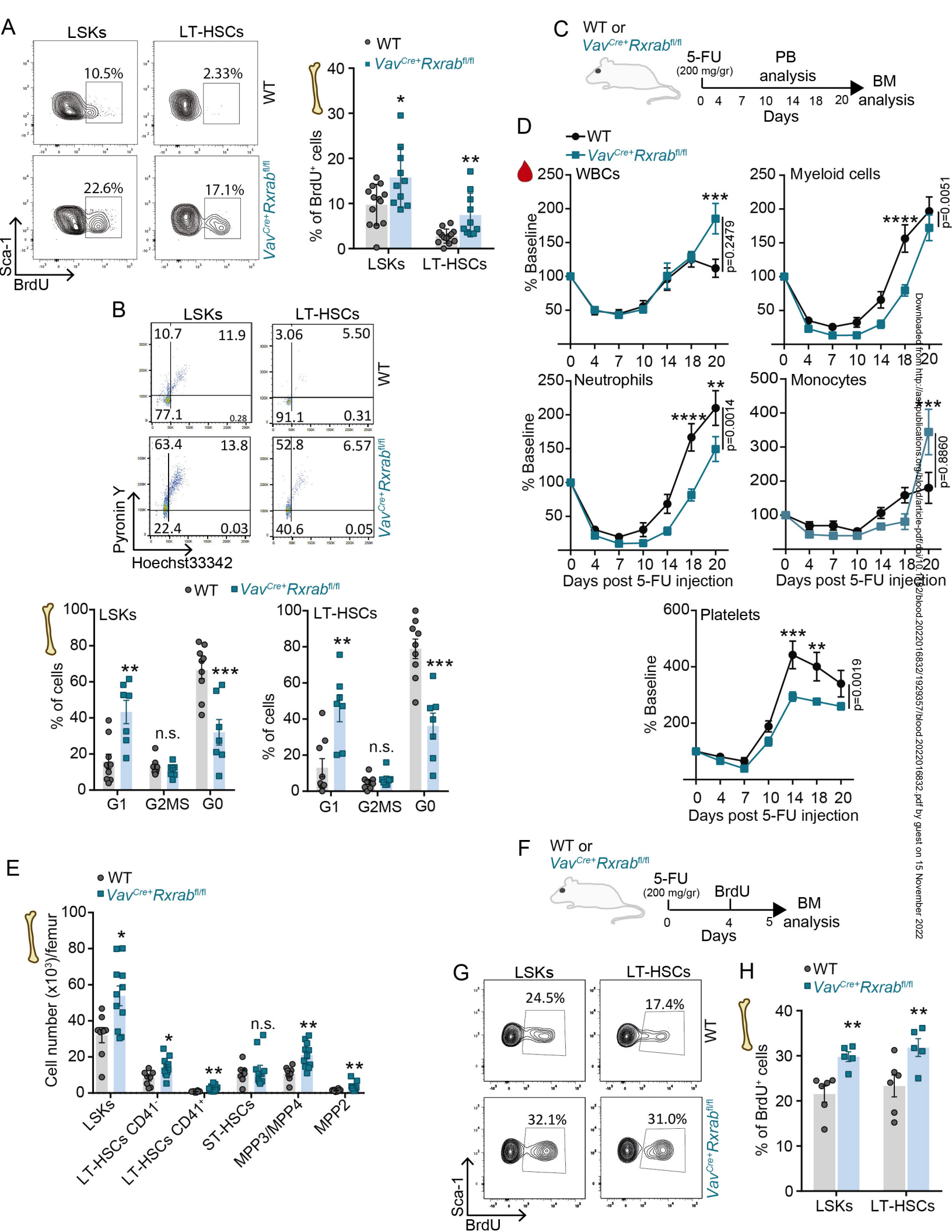

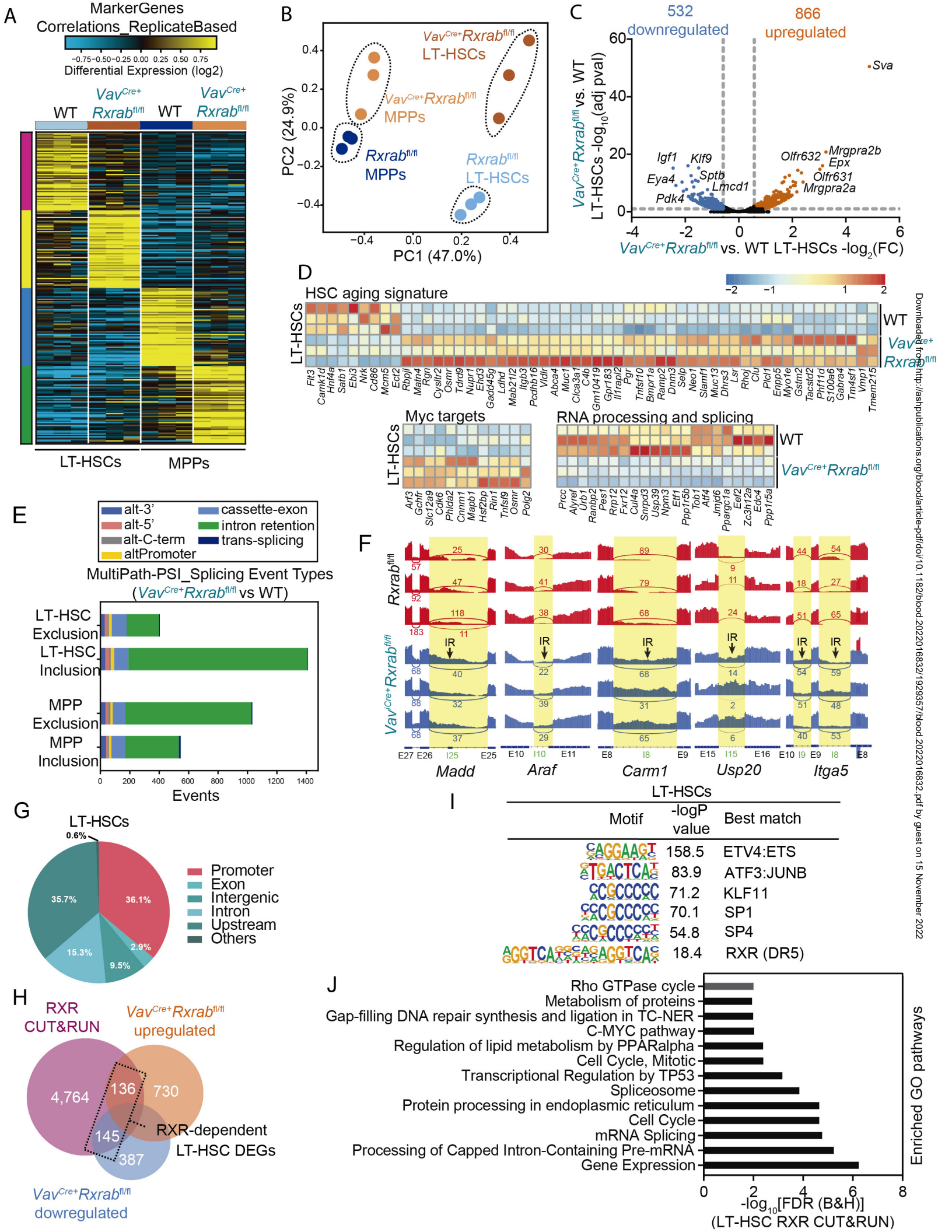

A

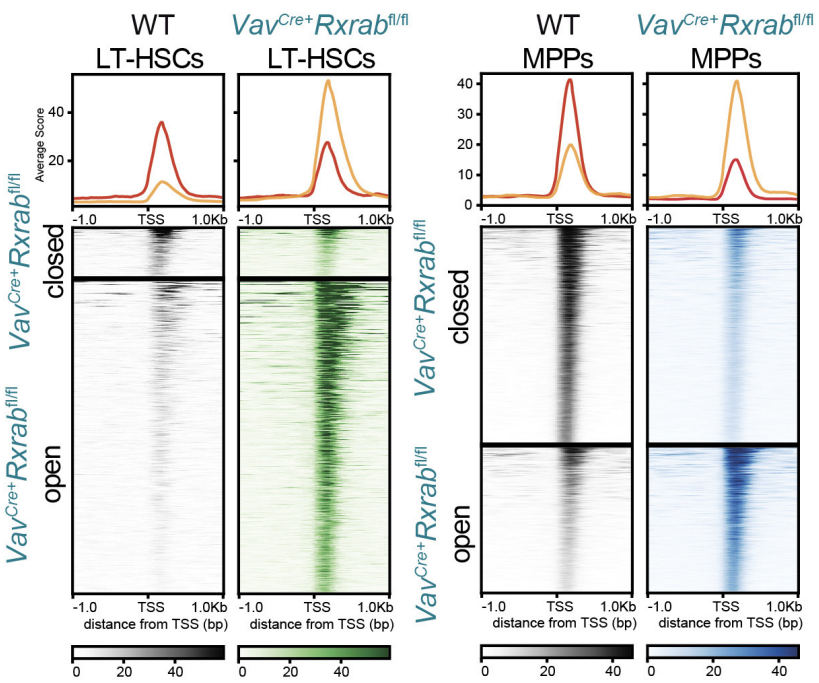

B

WT *vs* *Vav*$^{Cre+}$*Rxrab*$^{fl/fl}$ LT-HSCs

Motif	-logP value	Best match
	16	LXRE(NR),DR4
	9.9	THRa(NR)
	9.5	VDR(NR),DR3
	7.4	ETS1-distal(ETS)
	6.2	BACH1(bZIP)
	5.7	USF1(bHLH)
	5.5	RAR:RXR(NR),DR5
	5.2	CLOCK
	5.0	EWS:ERG-fusion

Vav^{Cre+}*Rxrab*$^{fl/fl}$ *vs* WT LT-HSCs

Motif	-logP value	Best match
	19.3	GATA2 (Zf)
	16.8	GATA1 (Zf)
	11.4	TGIF2
	9.5	GATA3 (Zf)
	8.2	IRF2
	8.1	MEIS1
	7.7	NFY (CCAAT)
	7.4	RUNX1
	7.2	OCT4
	6.9	PU.1/IRF
	5.4	HOX9A

C

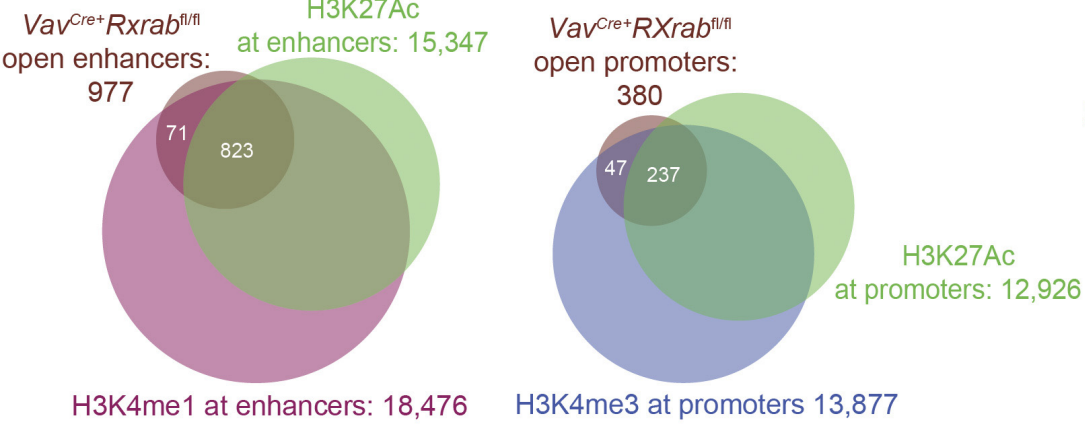

D